Accurate Passive Location Estimation Using TOA Measurements

Junyang Shen, Andreas F. Molisch, *Fellow, IEEE*, and Jussi Salmi, *Member, IEEE*

***Abstract*—Localization of objects is fast becoming a major aspect of wireless technologies, with applications in logistics, surveillance, and emergency response. Time-of-arrival (TOA) localization is ideally suited for high-precision localization of objects in particular in indoor environments, where GPS is not available. This paper considers the case where one transmitter and multiple, distributed, receivers are used to estimate the location of a passive (reflecting) object. It furthermore focuses on the situation when the transmitter and receivers can be synchronized, so that TOA (as opposed to time-difference-of-arrival (TDOA)) information can be used. We propose a novel, Two-Step estimation (TSE) algorithm for the localization of the object. We then derive the Cramer-Rao Lower Bound (CRLB) for TOA and show that it is an order of magnitude lower than the CRLB of TDOA in typical setups. The TSE algorithm achieves the CRLB when the TOA measurements are subject to small Gaussian-distributed errors, which is verified by analytical and simulation results. Moreover, practical measurement results show that the estimation error variance of TSE can be 33 dB lower than that of TDOA based algorithms.**

***Index Terms*—TOA, TDOA, location estimation, CRLB.**

I. Introduction

OBJECT location estimation has recently received intensive interests for a large variety of applications. For example, localization of people in smoke-filled buildings can be life-saving [1]; positioning techniques also provide useful location information for search-and-rescue [2], logistics [3], and security applications such as localization of intruders [4].

A variety of localization techniques have been proposed in the literature, which differ by the type of information and system parameters that are used. The three most important kinds utilize the received signal strength (RSS) [5], angle of arrival (AOA) [6], and signal propagation time [7], [8], [9], respectively. RSS algorithms use the received signal power for object positioning; their accuracies are limited by the fading of wireless signals [5]. AOA algorithms require either directional antennas or receiver antenna arrays [1]. Signal-propagation-time based algorithms estimate the object location using the time it takes the signal to travel from the transmitter to the target and from there to the receivers. They achieve very accurate estimation of object location if combined with high-precision timing measurement techniques [11], such as ultrawideband (UWB) signaling, which allows centimeter and even sub-millimeter accuracy, see [12], [13], and Section VII. Due to such merits, the UWB range determination is an ideal candidate for short-range object location systems and also forms the basis for the localization of sensor nodes in the IEEE 802.15.4a standard [14].

The algorithms based on signal propagation time can be further classified into Time of Arrival (TOA) and Time Difference of Arrival (TDOA). TOA algorithms employ the information of the *absolute* signal travel time from the transmitter to the target and thence to the receivers. The term "TOA" can be used in two different cases: 1) there is no synchronization between transmitters and receivers and then clock bias between them exist; 2) there is synchronization between transmitters and receivers and then clock bias between them does not exist. In this paper, we consider the second situation with the synchronization between the transmitter and receivers. Such synchronization can be done by cable connections between the devices, or sophisticated wireless synchronization algorithms [15]. TDOA is employed if there is no synchronization between the transmitter and the receivers. In that case, only the receivers are synchronized. Receivers do not know the signal travel time and therefore employ the *difference* of signal travel times between the receivers. It is intuitive that TOA has better performance than the TDOA, since the TDOA loses information about the signal departure time [7].

The TDOA/TOA positioning problems can furthermore be divided into "active" and "passive" object cases. "Active" means that the object itself is the transmitter, while "passive" means that it is not the transmitter nor receiver, but a separate (reflecting/scattering) object that just interacts with the signal stemming from a separate transmitter [2].

There are numerous papers on the TOA/TDOA location estimation for "active" objects. Regarding TDOA, the two-stage method [16] and the Approximate Maximum Likelihood Estimation [17] are shown to be able to achieve the Cramer-Rao Lower Bound (CRLB) of "active" TDOA [8]. As we know, the CRLB sets the lower bound of the estimation error variance of any un-biased method. Two important TOA methods of "active" object positioning are the Least-Square Method [18] and the Approximate Maximum Likelihood Estimation Method [17], both of which achieve the CRLB of "active" TOA. "Active" object estimation methods are used, e.g, for cellular handsets, WLAN, satellite positioning, and active RFID.

Manuscript received April 15, 2011; revised September 28, 2011 and January 18, 2012; accepted February 12, 2012. The associate editor coordinating the review of this paper and approving it for publication was X. Wang.

J. Shen and A. F. Molisch are, and J. Salmi was with the Department of Electrical Engineering, Viterbi School of Engineering, University of Southern California (e-mail: {junyangs, molisch, salmi}@usc.edu). J. Salmi is currently with Aalto University, SMARAD CoE, Espoo, Finland.

This paper is partially supported by the Office of Naval Research (ONR) under grant 10599363.

Part of this work was presented in the IEEE Int. Conference on Ultrawideband Communications 2011.

Digital Object Identifier 10.1109/TWC.2012.040412.110697

[1]Note that AOA does not provide better estimation accuracy than the signal propagation time based methods [10].

[2]The definitions of "active" and "passive" here are different from those in radar literature. In radar literature, "passive radar" does not transmit signals and only detects transmission while "active radar" transmits signals toward targets.

"Passive" positioning is necessary in many practical situations like crime-prevention surveillance, assets tracking, and medical patient monitoring, where the target to be localized is neither transmitter nor receiver, but a separate (reflecting/scattering) object. The TDOA positioning algorithms for "passive" objects are essentially the same as for "active" objects. For TOA, however, the synchronization creates a fundamental difference between "active" and "passive" cases. Regarding the "passive" object positioning, to the best of our knowledge, no TOA algorithms have been developed. This paper aims to fill this gap by proposing a TOA algorithm for **passive** object location estimation, which furthermore achieves the CRLB of "passive" TOA. The key contributions are:

- *A novel, two step estimation (TSE) method for the passive TOA based location estimation*. It borrows an idea from the TDOA algorithm of [16].
- *CRLB for passive TOA based location estimation*. When the TOA measurement error is Gaussian and small, we prove that the TSE can achieve the CRLB. Besides, it is also shown that the estimated target locations by TSE are Gaussian random variables whose covariance matrix is the inverse of the Fisher Information Matrix (FIM) related to the CRLB. We also show that in typical situations the CRLB of TOA is much lower than that of TDOA.
- *Experimental study of the performances of TSE*. With one transmitter and three receivers equipped with UWB antennas, we perform 100 experimental measurements with an aluminium pole as the target. After extracting the signal travel time by high-resolution algorithms, the location of the target is evaluated by TSE. We show that the variance of estimated target location by TSE is much (33dB) lower than that by the TDOA method in [16].

The remainder of this paper is organized as follows. Section II presents the architecture of positioning system. Section III derives the TSE, followed by comparison between CRLB of TOA and TDOA algorithms in Section IV. Section V analyzes the performance of TSE. Section VI presents the simulations results. Section VII evaluates the performance of TSE based on UWB measurement. Finally Section VIII draws the conclusions.

Notation: Throughout this paper, a variable with "hat" $\hat{\bullet}$ denotes the measured/estimated values, and the "bar" $\bar{\bullet}$ denotes the mean value. Bold letters denote vectors/matrices. $E(\bullet)$ is the expectation operator. If not particularly specified, "TOA" in this paper denotes the "TOA" for a passive object.

II. Architecture of Localization System

In this section, we first discuss the challenges of localization systems, and present the focus of this paper. Then, the system model of individual localization is discussed.

A. Challenges for target localization

For easy understanding, we consider an intruder localization system using UWB signals. Note that the intruder detection can also be performed using other methods such as the Device-free Passive (DfP) approach [19] and Radio Frequency Identification (RFID) method [20]. However, both the DfP and RFID methods are based on preliminary environmental measurement information like "Radio Map Construction" [19] and "fingerprints" [20]. On the other hand, the TOA based approach considered in our framework does not require the preliminary efforts for obtaining environmental information.

With this example, we show the challenges of target positioning system: Multiple Source Separation, Indirect Path Detection and Individual Target Localization.

The intruder detection system localizes, and then directs a camera to capture the photo of the targets (intruders). This localization system consists of one transmitter and several receivers. The transmitter transmits signals which are reflected by the targets, then, the receivers localize the targets based on the received signals.

Multiple Source Separation: If there are more than one intruders, the system needs to localize each of them. With multiple targets, each receiver receives impulses from several objects. Only the information (such as TOA) extracted from impulses reflected by the same target should be combined for localization. Thus, the Multiple Source Separation is very important for target localization and several techniques have been proposed for this purpose. In [21], a pattern recognition scheme is used to perform the Multiple Source Separation. Video imaging and blind source separation techniques are employed for target separation in [22].

Indirect Path Detection: The transmitted signals are not only reflected by the intruders, but also by surrounding objects, such as walls and tables. To reduce the adverse impact of non-target objects in the localization of target, the localization process consists of two steps. In the initial/first stage, the system measures and then stores the channel impulses without the intruders. These impulses are reflected by non-target objects, which is referred to as reflectors here. The radio signal paths existing without the target are called background paths. When the intruders are present, the system performs the second measurement. To obtain the impulses related to the intruders, the system subtracts the second measurement with the first one. The remaining impulses after the subtraction can be through one of the following paths: a) transmitter-intruders-receivers, b) transmitter-reflectors-intruders-receivers, c) transmitter-intruders-reflectors-receivers, d) transmitter-reflectors-intruders-reflectors-receivers[3]. The first kind of paths are called direct paths and the rest are called indirect paths. In most situations, only direct paths can be used for localization. In the literature, there are several methods proposed for indirect path identification [23], [24].

Individual Target Localization: After the Multiple Source Separation and Indirect Path Detection, the positioning system knows the signal impulses through the direct paths for each target. Then, the system extracts the characteristics of direct paths such as TOA and AOA. Based on these characteristics, the targets are finally localized. Most researches on Individual Target Localization assumes that Multiple Source Separation and Indirect Path Detection are perfectly performed such as [16], [25] and [26]. Note that the three challenges sometimes

[3]Note that here we omit the impulses having two or more interactions with the intruder because of the resulted low signal-to-noise radio (SNR) by multiple reflections.

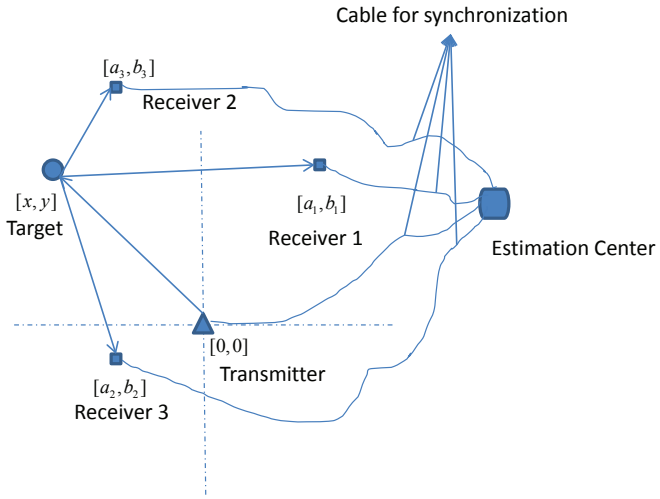

Fig. 1. Illustration of TOA based Location Estimation System Model.

are jointly addressed, so that the target locations are estimated in one step such as the method presented in [27].

In this paper, we focus on the Individual Target Localization, under the same framework of [16], [25] and [26], assuming that Multiple Source Separation and Indirect Path Detection are perfectly performed in prior. In addition, we only use the TOA information for localization, which achieves very high accuracy with ultra-wideband signals. The method to extract TOA information using background channel cancelation is described in details in [28] and also Section VII.

B. System Model of Individual Localization

For ease of exposition, we consider the passive object (target) location estimation problem in a two-dimensional plane as shown in Fig. 1. There is a target whose location $[x, y]$ is to be estimated by a system with one transmitter and M receivers. Without loss of generality, let the location of the transmitter be $[0, 0]$, and the location of the ith receiver be $[a_i, b_i]$, $1 \le i \le M$. The transmitter transmits an impulse; the receivers subsequently receive the signal copies reflected from the target and other objects. We adopt the assumption also made in [16], [17] that the target reflects the signal into all directions. Using (wired) backbone connections between the transmitter and receivers, or high-accuracy wireless synchronization algorithms, the transmitter and receivers are synchronized. The errors of cable synchronization are negligible compared with the TOA measurement errors. Thus, at the estimation center, signal travel times can be obtained by comparing the departure time at the transmitter and the arrival time at the receivers.

Let the TOA from the transmitter via the target to the ith receiver be t_i, and $r_i = c_0 t_i$, where c_0 is the speed of light, $1 \le i \le M$. Then,

$$r_i = \sqrt{x^2 + y^2} + \sqrt{(x - a_i)^2 + (y - b_i)^2} \quad i = 1, ...M. \quad (1)$$

For future use we define $\mathbf{r} = [r_1, r_2, \ldots, r_M]$. Assuming each measurement involves an error, we have

$$r_i - \hat{r}_i = e_i, \qquad 1 \le i \le M,$$

where r_i is the true value, $\hat{r}_i$ is the measured value and e_i is the measurement error. In our model, the indirect paths are ignored and we assume e_i to be zero mean. The estimation system tries to find the $[\hat{x}, \hat{y}]$, that best fits the above equations in the sense of minimizing the error variance

$$\Delta = E[(\hat{x} - x)^2 + (\hat{y} - y)^2]. \quad (2)$$

Assuming the e_i are Gaussian-distributed variables with zero mean and variances σ_i^2, the conditional probability function of the observations $\hat{\mathbf{r}}$ are formulated as follows:

$$p(\hat{\mathbf{r}}|\mathbf{z}) = \prod_{i=1}^{N} \frac{1}{\sqrt{2\pi}\sigma_i} \cdot \exp\Bigg(- \frac{(\hat{r}_i - (\sqrt{x^2 + y^2} + \sqrt{(x - a_i)^2 + (y - b_i)^2}))^2}{2\sigma_i^2} \Bigg), \quad (3)$$

where $\mathbf{z} = [x, y]$.

III. TSE Method

In this section, we present the two steps of TSE and summarize them in Algorithm 1. In the first step of TSE, we assume x, y, $\sqrt{x^2 + y^2}$ are independent of each other, and obtain temporary results for the target location based on this assumption. In the second step, we remove the assumption and update the estimation results.

A. Step 1 of TSE

In the first step of TSE, we obtain an initial estimate of $[x, y, \sqrt{x^2 + y^2}]$, which is performed in two stages: Stage A and Stage B. The basic idea here is to utilize the linear approximation [16] [29] to simplify the problem, considering that TOA measurement errors are small with UWB signals.

Let $v = \sqrt{x^2 + y^2}$, taking the squares of both sides of (1) leads to

$$2a_i x + 2b_i y - 2r_i v = a_i^2 + b_i^2 - r_i^2.$$

Since $r_i - \hat{r}_i = e_i$, it follows that

$$\begin{aligned} &- \frac{a_i^2 + b_i^2 - \hat{r}_i^2}{2} + a_i x + b_i y - \hat{r}_i v \\ &= e_i(v - \hat{r}_i) - \frac{e_i^2}{2} = e_i(v - \hat{r}_i) - \mathcal{O}(e_i^2). \end{aligned} \quad (4)$$

where $\mathcal{O}(\bullet)$ is the *Big $\mathcal{O}$ Notation* meaning that $f(\alpha) = \mathcal{O}(g(\alpha))$ if and only if there exits a positive real number M and a real number α such that

$$|f(\alpha)| \le M|g(\alpha)| \text{ for all } \alpha > \alpha_0.$$

If e_i is small, we can omit the second or higher order terms $\mathcal{O}(e_i^2)$ in Eqn (4). In the following of this paper, we do this, leaving the linear (first order) term. Since there are M such equations, we can express them in a matrix form as follows

$$\mathbf{h} - \mathbf{S}\boldsymbol{\theta} = \mathbf{B}\mathbf{e} + \mathcal{O}(\mathbf{e}^2) \approx \mathbf{B}\mathbf{e}, \quad (5)$$

where

$$\mathbf{h} = \begin{bmatrix} -\frac{a_1^2+b_1^2-\hat{r}_1^2}{2} \\ -\frac{a_2^2+b_2^2-\hat{r}_2^2}{2} \\ \vdots \\ -\frac{a_M^2+b_M^2-\hat{r}_M^2}{2} \end{bmatrix},$$

$$\mathbf{S} = -\begin{bmatrix} a_1 & b_1 & -\hat{r}_1 \\ a_2 & b_2 & -\hat{r}_2 \\ & \vdots & \\ a_M & b_M & -\hat{r}_M \end{bmatrix},$$

$$\boldsymbol{\theta} = [x, y, v]^T,$$

$$\mathbf{e} = [e_1, e_2, \ldots, e_M]^T,$$

and

$$\mathbf{B} = v \cdot \mathbf{I} - \text{diag}\left([r_1, r_2, \ldots, r_M]\right), \tag{6}$$

where $\mathcal{O}(\mathbf{e}^2) = [\mathcal{O}(e_1^2), \mathcal{O}(e_2^2), ..., \mathcal{O}(e_M^2)]^T$ and $\text{diag}(\mathbf{a})$ denotes the diagonal matrix with elements of vector $\mathbf{a}$ on its diagonal. For notational convenience, we define the error vector

$$\boldsymbol{\varphi} = \mathbf{h} - \mathbf{S}\boldsymbol{\theta}. \tag{7}$$

According to (5) and (7), the mean of $\boldsymbol{\varphi}$ is zero, and its covariance matrix is given by

$$\begin{aligned} \boldsymbol{\Psi} &= E(\boldsymbol{\varphi}\boldsymbol{\varphi}^T) \\ &= E(\mathbf{B}\mathbf{e}\mathbf{e}^T\mathbf{B}^T) + E(\mathcal{O}(\mathbf{e}^2)\mathbf{e}^T\mathbf{B}^T) \\ &\quad + E(\mathbf{B}\mathbf{e}\mathcal{O}(\mathbf{e}^2)^T) + E(\mathcal{O}(\mathbf{e}^2)\mathcal{O}(\mathbf{e}^2)^T) \\ &\approx \bar{\mathbf{B}}\mathbf{Q}\bar{\mathbf{B}}^T \end{aligned} \tag{8}$$

where $\mathbf{Q} = \text{diag}\ [\sigma_1^2, \sigma_2^2, \ldots, \sigma_M^2]$. Because $\bar{\mathbf{B}}$ depends on the true values $\mathbf{r}$, which are not obtainable, we use $\widehat{\mathbf{B}}$ (derived from the measurements $\hat{\mathbf{r}}$) in our calculations.

From (5) and the definition of $\boldsymbol{\varphi}$, it follows that $\boldsymbol{\varphi}$ is a vector of Gaussian variables; thus, the probability density function (pdf) of $\boldsymbol{\varphi}$ given $\boldsymbol{\theta}$ is

$$\begin{aligned} p(\boldsymbol{\varphi}|\boldsymbol{\theta}) &\approx \frac{1}{(2\pi)^{\frac{M}{2}}|\boldsymbol{\Psi}|^{\frac{1}{2}}} \exp(-\frac{1}{2}\boldsymbol{\varphi}^T\boldsymbol{\Psi}^{-1}\boldsymbol{\varphi}) \\ &= \frac{1}{(2\pi)^{\frac{M}{2}}|\boldsymbol{\Psi}|^{\frac{1}{2}}} \exp(-\frac{1}{2}(\mathbf{h}-\mathbf{S}\boldsymbol{\theta})^T\boldsymbol{\Psi}^{-1}(\mathbf{h}-\mathbf{S}\boldsymbol{\theta})). \end{aligned}$$

Then,

$$\begin{aligned} \ln\left(p(\boldsymbol{\varphi}|\boldsymbol{\theta})\right) \approx & -\frac{1}{2}\Big((\mathbf{h}-\mathbf{S}\boldsymbol{\theta})^T\boldsymbol{\Psi}^{-1}(\mathbf{h}-\mathbf{S}\boldsymbol{\theta}) \\ & + \ln|\boldsymbol{\Psi}|\Big) - \frac{M}{2}\ln 2\pi \end{aligned} \tag{9}$$

We *assume* for the moment that x, y, v are independent of each other (this clearly non-fulfilled assumption will be relaxed in the second step of the algorithm). Then, according to (9), the optimum $\boldsymbol{\theta}$ that maximizes $p(\boldsymbol{\varphi}|\boldsymbol{\theta})$ is equivalent to the one minimizing $\Pi = (\mathbf{h}-\mathbf{S}\boldsymbol{\theta})^T\boldsymbol{\Psi}^{-1}(\mathbf{h}-\mathbf{S}\boldsymbol{\theta}) + \ln|\boldsymbol{\Psi}|$. If $\boldsymbol{\Psi}$ is a constant, the optimum $\boldsymbol{\theta}$ to minimize Π satisfies $\frac{d\Pi}{d\boldsymbol{\theta}} = 0$. Taking the derivative of Π over $\boldsymbol{\theta}$, we have

$$\frac{d\Pi}{d\boldsymbol{\theta}} = -2\mathbf{S}^T\boldsymbol{\Psi}^{-1}\mathbf{h} + 2\mathbf{S}^T\boldsymbol{\Psi}^{-1}\mathbf{S}\boldsymbol{\theta}.$$

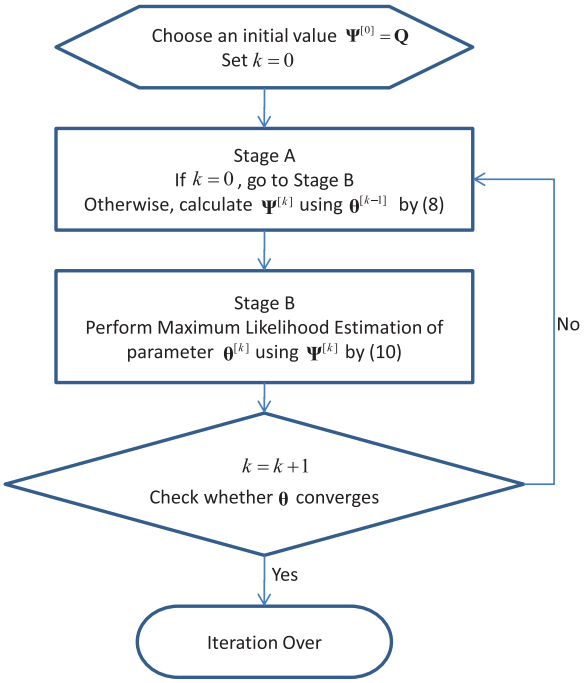

Fig. 2. Illustration of estimation of $\boldsymbol{\theta}$ in step 1 of TSE.

Thus, the optimum $\boldsymbol{\theta}$ satisfies

$$\hat{\boldsymbol{\theta}} = \arg\min_{\boldsymbol{\theta}}\{\Pi\} = (\mathbf{S}^T\boldsymbol{\Psi}^{-1}\mathbf{S})^{-1}\mathbf{S}^T\boldsymbol{\Psi}^{-1}\mathbf{h}, \tag{10}$$

which provides $[\hat{x}, \hat{y}]$. Note that (10) also provides the least squares solution for non-Gaussian errors.

However, for our problem, $\boldsymbol{\Psi}$ is a function of $\boldsymbol{\theta}$ since $\mathbf{B}$ depends on the (unknown) values $[x, y]$. For this reason, the maximum-likelihood (ML) estimation method in (10) can not be directly used. To find the optimum $\boldsymbol{\theta}$, we perform the estimation in two stages: Stage A and Stage B. In Stage A, the missing data ($\boldsymbol{\Psi}$) is calculated given the estimate of parameters ($\boldsymbol{\theta}$). Note that $\boldsymbol{\theta}$ provides the values of $[x, y]$ and thus the value of $\widehat{\mathbf{B}}$, therefore, $\boldsymbol{\Psi}$ can be calculated using $\boldsymbol{\theta}$ by (8). In the Stage B, the parameters ($\boldsymbol{\theta}$) are updated according to (10) to maximize the likelihood function (which is equivalent to minimizing Π). These two stages are iterated until convergence. Simulations in Section V show that commonly one iteration is enough for TSE to closely approach the CRLB, which indicates that the global optimum is reached.

B. Step 2 of TSE

In the above calculations, $\hat{\boldsymbol{\theta}}$ contains three components $\hat{x}$, $\hat{y}$ and $\hat{v}$. They were previously assumed to be independent; however, $\hat{x}$ and $\hat{y}$ are clearly not independent of $\hat{v}$. As a matter of fact, we wish to eliminate $\hat{v}$; this will be achieved by treating $\hat{x}$, $\hat{y}$, and $\hat{v}$ as random variables, and, knowing the linear mapping of their squared values, the problem can be solved using the LS solution. Let

$$\hat{\boldsymbol{\theta}} = \begin{bmatrix} \hat{x} \\ \hat{y} \\ \hat{v} \end{bmatrix} = \begin{bmatrix} x+n_1 \\ y+n_2 \\ v+n_3 \end{bmatrix} \tag{11}$$

where n_i $(i = 1, 2, 3)$ are the estimation errors of the first step. Obviously, the estimator (10) is an unbiased one, and the

mean of n_i is zero. Before proceeding, we need the following Lemma.

Lemma 1: By omitting the second or higher order errors, the covariance of $\hat{\boldsymbol{\theta}}$ can be approximated as

$$\text{cov}(\hat{\boldsymbol{\theta}}) = E(\mathbf{n}\mathbf{n}^T) \approx (\bar{\mathbf{S}}^T \boldsymbol{\Psi}^{-1} \bar{\mathbf{S}})^{-1}. \quad (12)$$

where $\mathbf{n} = [n_1, n_2, n_3]^T$, and $\boldsymbol{\Psi}$ and $\bar{\mathbf{S}}$ (the mean value of $\mathbf{S}$) use the true/mean values of x, y, and r_i.

Proof: Please refer to the Appendix. ■

Note that since the true values of x, y, and r_i are not obtainable, we use the estimated/measured values in the calculation of $\text{cov}(\hat{\boldsymbol{\theta}})$.

Let us now construct a vector $\mathbf{g}$ as follows

$$\mathbf{g} = \hat{\boldsymbol{\Theta}} - \mathbf{G}\Upsilon, \quad (13)$$

where $\hat{\boldsymbol{\Theta}} = [\hat{x}^2, \hat{y}^2, \hat{v}^2]^T$, $\Upsilon = [x^2, y^2]^T$ and

$$\mathbf{G} = \begin{bmatrix} 1 & 0 \\ 0 & 1 \\ 1 & 1 \end{bmatrix}.$$

Note that here $\hat{\boldsymbol{\Theta}}$ is the square of estimation result $\hat{\boldsymbol{\theta}}$ from the first step containing the estimated values $\hat{x}$, $\hat{y}$ and $\hat{v}$. Υ is the vector to be estimated. If $\hat{\boldsymbol{\Theta}}$ is obtained without error, $\mathbf{g} = 0$ and the location of the target is perfectly obtained. However, the error inevitably exists and we need to estimate Υ. Recalling that $v = \sqrt{x^2 + y^2}$, substituting (11) into (13), and omitting the second-order terms n_1^2, n_2^2, n_3^2, it follows that,

$$\mathbf{g} = \begin{bmatrix} 2xn_1 + \mathcal{O}(n_1^2) \\ 2yn_2 + \mathcal{O}(n_2^2) \\ 2vn_3 + \mathcal{O}(n_3^2) \end{bmatrix} \approx \begin{bmatrix} 2xn_1 \\ 2yn_2 \\ 2vn_3 \end{bmatrix}.$$

Besides, following similar procedure as that in computing (8), we have

$$\boldsymbol{\Omega} = E(\mathbf{g}\mathbf{g}^T) \approx 4\bar{\mathbf{D}}\text{cov}(\hat{\boldsymbol{\theta}})\bar{\mathbf{D}}, \quad (14)$$

where $\bar{\mathbf{D}} = \text{diag}([\bar{x}, \bar{y}, \bar{v}])$. Since x, y are not known, $\bar{\mathbf{D}}$ is calculated as $\hat{\mathbf{D}}$ using the estimated values $\hat{x}$, $\hat{y}$ from the first step. The vector $\mathbf{g}$ can be approximated as a vector of Gaussian variables. Thus the maximum likelihood estimation of Υ is the one minimizing $(\hat{\boldsymbol{\Theta}} - \mathbf{G}\Upsilon)^T \boldsymbol{\Omega}^{-1} (\hat{\boldsymbol{\Theta}} - \mathbf{G}\Upsilon)$, expressed by

$$\hat{\Upsilon} = (\mathbf{G}^T \boldsymbol{\Omega}^{-1} \mathbf{G})^{-1} \mathbf{G}^T \boldsymbol{\Omega}^{-1} \hat{\boldsymbol{\Theta}}. \quad (15)$$

The value of $\boldsymbol{\Omega}$ is calculated according to (14) using the values of $\hat{x}$ and $\hat{y}$ in the first step. Finally, the estimation of target location $\mathbf{z}$ is obtained by

$$\hat{\mathbf{z}} = [\hat{x}, \hat{y}] = [\pm\sqrt{\hat{\Upsilon}_1}, \pm\sqrt{\hat{\Upsilon}_2}], \quad (16)$$

where $\hat{\Upsilon}_i$is the ith item of Υ, $i = 1, 2$. To choose the correct one among the four values in (16), we can test the square error as follows

$$\chi = \sum_{i=1}^{M} (\sqrt{\hat{x}^2 + \hat{y}^2} + \sqrt{(\hat{x} - a_i)^2 + (\hat{y} - b_i)} - \hat{r}_i)^2. \quad (17)$$

The value of $\mathbf{z}$ that minimizes χ is considered as the final estimate of the target location.

In summary, the procedure of TSE is listed in Algorithm 1:

Note that one should avoid placing the receivers on a line, since in this case $(\mathbf{S}^T \boldsymbol{\Psi}^{-1} \mathbf{S})^{-1}$ can become nearly singular, and solving (10) is not accurate.

Algorithm 1 TSE Location Estimation Method

1. In the first step, use algorithm as shown in Fig. 2 to obtain $\hat{\boldsymbol{\theta}}$,
2. In the second step, use the values of $\hat{x}$ and $\hat{y}$ from $\hat{\boldsymbol{\theta}}$, generate $\hat{\boldsymbol{\Theta}}$ and $\mathbf{D}$, and calculate $\boldsymbol{\Omega}$. Then, calculate the value of $\hat{\Upsilon}$ by (15),
3. Among the four candidate values of $\hat{\mathbf{z}} = [\hat{x}, \hat{y}]$ obtained by (16), choose the one minimizing (17) as the final estimate for target location.

IV. Comparison of CRLB between TDOA and TOA

In this section, we derive the CRLB of TOA based estimation algorithms and show that it is much lower (can be 30 dB lower) than the CRLB of TDOA algorithms.

The CRLB of "active" TOA localization has been studied in [30]. The "passive" localization has been studied before under the model of multistatic radar [31], [32], [33]. The difference between our model and the radar model is that in our model the localization error is a function of errors of TOA measurements, while in the radar model the localization error is a function of signal SNR and waveform.

The CRLB is related to the 2×2 Fisher Information Matrix (FIM) [34], $\mathbf{J}$, whose components $J_{11}, J_{12}, J_{21}, J_{22}$ are defined in (18) – (20) as follows

$$J_{11} = -E(\frac{\partial^2 \ln(p(\hat{\mathbf{r}}|\mathbf{z}))}{\partial x^2}) = \Sigma_{i=1}^{M} \frac{1}{\sigma_i^2} (\frac{x - a_i}{\sqrt{(x - a_i)^2 + (y - b_i)^2}} + \frac{x}{\sqrt{x^2 + y^2}})^2, \quad (18)$$

$$J_{12} = J_{21} = -E(\frac{\partial^2 \ln(p(\hat{\mathbf{r}}|\mathbf{z}))}{\partial x \partial y}) = \Sigma_{i=1}^{M} \frac{1}{\sigma_i^2} (\frac{x - a_i}{\sqrt{(x - a_i)^2 + (y - b_i)^2}} + \frac{x}{\sqrt{x^2 + y^2}}) \times (\frac{y - b_i}{\sqrt{(x - a_i)^2 + (y - b_i)^2}} + \frac{y}{\sqrt{x^2 + y^2}}), \quad (19)$$

$$J_{22} = -E(\frac{\partial^2 \ln(p(\hat{\mathbf{r}}|\mathbf{z}))}{\partial y^2}) = \Sigma_{i=1}^{M} \frac{1}{\sigma_i^2} (\frac{y - b_i}{\sqrt{(x - a_i)^2 + (y - b_i)^2}} + \frac{y}{\sqrt{x^2 + y^2}})^2. \quad (20)$$

This can be expressed as

$$\mathbf{J} = \mathbf{U}^T \mathbf{Q}^{-1} \mathbf{U}, \quad (21)$$

where $\mathbf{Q}$ is defined after Eqn. (8), and the entries of $\mathbf{U}$ in the first and second column are

$$\{\mathbf{U}\}_{i,1} = \frac{x\bar{r}_i - a_i\sqrt{x^2 + y^2}}{\sqrt{(x - a_i)^2 + (y - b_i)^2}\sqrt{x^2 + y^2}}, \quad (22)$$

and

$$\{\mathbf{U}\}_{i,2} = \frac{y\bar{r}_i - b_i\sqrt{x^2 + y^2}}{\sqrt{(x - a_i)^2 + (y - b_i)^2}\sqrt{x^2 + y^2}}, \quad (23)$$

with $\bar{r}_i = \sqrt{(x - a_i)^2 + (y - b_i)^2} + \sqrt{x^2 + y^2}$.

The CRLB sets the lower bound for the variance of estimation error of TOA algorithms, which can be expressed as [34]

$$E[(\hat{x}-x)^2+(\hat{y}-y)^2] \geq \left\{\mathbf{J}^{-1}\right\}_{1,1}+\left\{\mathbf{J}^{-1}\right\}_{2,2} = CRLB_{TOA}, \tag{24}$$

where $\hat{x}$ and $\hat{y}$ are the estimated values of x and y, respectively, and $\left\{\mathbf{J}^{-1}\right\}_{i,j}$ is the $(i,j)^{th}$ element of the inverse matrix of $\mathbf{J}$ in (21).

For the TDOA estimation, its CRLB has been derived in [16]. The difference of signal travel time between several receivers are considered:

$$\begin{aligned}&\sqrt{(x-a_i)^2+(y-b_i)^2}-\sqrt{(x-a_1)^2+(y-b_1)^2}\\&=r_i-r_1=l_i, \quad 2\leq i\leq M.\end{aligned} \tag{25}$$

Let $\mathbf{l} = [l_2, l_3, \ldots, l_M]^T$, and $\mathbf{t}$ be the observations/measurements of $\mathbf{l}$, then, the conditional probability density function of $\mathbf{t}$ is

$$p(\mathbf{t}|\mathbf{z})=\frac{1}{(2\pi)^{(M-1)/2}|\mathbf{Z}|^{\frac{1}{2}}}\times\exp(-\frac{1}{2}(\mathbf{t}-\mathbf{l})^T\mathbf{Z}^{-1}(\mathbf{t}-\mathbf{l})),$$

where $\mathbf{Z}$ is the correlation matrix of $\mathbf{t}$,

$$\mathbf{Z} = E(\mathbf{t}\mathbf{t}^T).$$

Then, the FIM is expressed as [16]

$$\check{\mathbf{J}} = \check{\mathbf{U}}^T\mathbf{Z}^{-1}\check{\mathbf{U}} \tag{26}$$

where $\check{\mathbf{U}}$ is a $M-1\times 2$ matrix defined as

$$\check{\mathbf{U}}_{i,1} = \frac{x-a_i}{\sqrt{(x-a_i)^2+(y-b_i)^2}}-\frac{x-a_1}{\sqrt{(x-a_1)^2+(y-b_1)^2}},$$

$$\check{\mathbf{U}}_{i,2} = \frac{y-b_i}{\sqrt{(x-a_i)^2+(y-b_i)^2}}-\frac{y-b_1}{\sqrt{(x-a_1)^2+(y-b_1)^2}}.$$

The CRLB sets the lower bound for the variance of estimation error of TDOA algorithms, which can be expressed as [34]:

$$E[(\hat{x}-x)^2+(\hat{y}-y)^2] \geq \left\{\check{\mathbf{J}}^{-1}\right\}_{1,1}+\left\{\check{\mathbf{J}}^{-1}\right\}_{2,2} = CRLB_{TDOA}. \tag{27}$$

Note that the correlation matrix $\mathbf{Q}$ for TOA is different from the correlation matrix $\mathbf{Z}$ for TDOA. Assume the variance of TOA measurement at ith $(1 \leq i \leq M)$ receiver is σ_i^2, it follows that:

$$\mathbf{Q}(i,j) = \begin{cases}\sigma_i^2 & i=j,\\ 0 & i\neq j.\end{cases}$$

and

$$\mathbf{Z}(i,j) = \begin{cases}\sigma_1^2+\sigma_{i+1}^2 & i=j,\\ \sigma_1^2 & i\neq j.\end{cases}$$

As an example, we consider a scenario where there is a transmitter at $[0, 0]$, and four receivers at $[-6, 2], [6.2, 1.4], [1.5, 4], [2, 2.3]$. The range of the target locations is $1 \leq x \leq 10$, $1 \leq y \leq 10$. The ratio of CRLB of TOA over that of TDOA is plotted in Fig. 3. Fig. 3 (a) shows the contour plot while Fig. 3 (b) shows the color-coded plot. It can be observed that the CRLB of TOA is always — in most cases significantly — lower than that of TDOA.

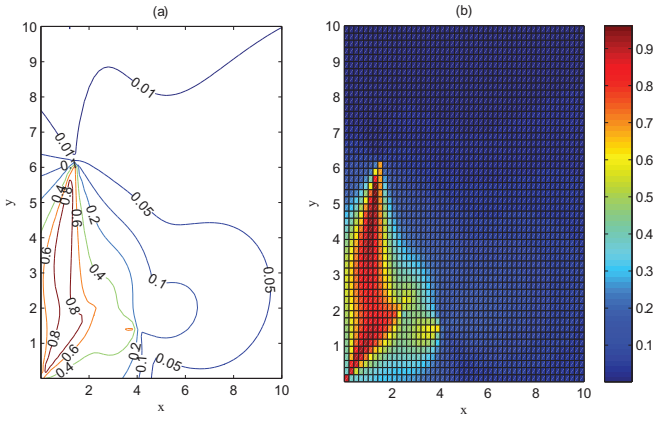

Fig. 3. CRLB ratio of passive TOA over passive TDOA estimation: (a) contour plot; (b) pcolor plot.

V. Performance of TSE

In this section, we first prove that the TSE can achieve the CRLB of TOA algorithms by showing that the estimation error variance of TSE is the same as the CRLB of TOA algorithms. In addition, we show that, for small TOA error regions, the estimated target location is approximately a Gaussian random variable whose covariance matrix is the inverse of the Fisher Information Matrix (FIM), which in turn is related to the CRLB.

Similar to the reasoning in Lemma 1, we can obtain the variance of error in the estimation of Υ as follows:

$$\text{cov}(\hat{\Upsilon}) \approx (\mathbf{G}^T\mathbf{\Omega}^{-1}\mathbf{G})^{-1}. \tag{28}$$

Let $\hat{x} = x+e_x$, $\hat{y} = y+e_y$, and insert them into Υ, omitting the second order errors, we obtain

$$\begin{aligned}\hat{\Upsilon}_1 - x^2 &= 2xe_x + \mathcal{O}(e_x^2) \approx 2xe_x\\ \hat{\Upsilon}_2 - y^2 &= 2ye_y + \mathcal{O}(e_y^2) \approx 2ye_y\end{aligned} \tag{29}$$

Then, the variance of the final estimate of target location $\hat{\mathbf{z}}$ is

$$\begin{aligned}\text{cov}(\hat{\mathbf{z}}) &= E(\begin{bmatrix}e_x\\ e_y\end{bmatrix}\begin{bmatrix}e_x & e_y\end{bmatrix})\\ &\approx \frac{1}{4}\mathbf{C}^{-1}E(\begin{bmatrix}\Upsilon_1-x^2\\ \Upsilon_2-y^2\end{bmatrix}\begin{bmatrix}\Upsilon_1-x^2 & \Upsilon_2-y^2\end{bmatrix})\mathbf{C}^{-1}\\ &= \frac{1}{4}\mathbf{C}^{-1}\text{cov}(\hat{\Upsilon})\mathbf{C}^{-1},\end{aligned} \tag{30}$$

where

$$\mathbf{C} = \begin{bmatrix}x & 0\\ 0 & y\end{bmatrix}.$$

Substituting (14), (28), (12) and (8) into (30), we can rewrite $\text{cov}(\hat{\mathbf{z}})$ as

$$\text{cov}(\hat{\mathbf{z}}) \approx (\mathbf{W}^T\mathbf{Q}^{-1}\mathbf{W})^{-1} \tag{31}$$

where $\mathbf{W} = \mathbf{B}^{-1}\bar{\mathbf{S}}\mathbf{D}^{-1}\mathbf{G}\mathbf{C}$. Since we are computing an error variance, $\mathbf{B}$ (19), $\bar{\mathbf{S}}$ (5) and $\mathbf{D}$ (14) are calculated using the true (mean) value of x, y and r_i. Using (19) and (1), we can rewrite $\mathbf{B} = -\text{diag}\,([d_1, d_2, \ldots, d_M])$, where

$d_i = \sqrt{(x-a_i)^2+(y-b_i)^2}$. Then $\mathbf{B}^{-1}\bar{\mathbf{S}}\mathbf{D}^{-1}$ is given by

$$\mathbf{B}^{-1}\bar{\mathbf{S}}\mathbf{D}^{-1} = \begin{bmatrix} \frac{a_1}{xd_1} & \frac{b_1}{yd_1} & \frac{-\bar{r}_1}{\sqrt{x^2+y^2}d_1} \\ \frac{a_2}{xd_2} & \frac{b_2}{yd_2} & \frac{-\bar{r}_2}{\sqrt{x^2+y^2}d_2} \\ \vdots & \vdots & \vdots \\ \frac{a_M}{xd_M} & \frac{b_M}{yd_M} & \frac{-\bar{r}_M}{\sqrt{x^2+y^2}d_M} \end{bmatrix}. \quad (32)$$

Consequently, we obtain the entries of $\mathbf{W}$ as

$$\{\mathbf{W}\}_{i,1} = \frac{x\bar{r}_i - a_i\sqrt{x^2+y^2}}{\sqrt{(x-a_i)^2+(y-b_i)^2}\sqrt{x^2+y^2}}, \quad (33)$$

$$\{\mathbf{W}\}_{i,2} = \frac{y\bar{r}_i - b_i\sqrt{x^2+y^2}}{\sqrt{(x-a_i)^2+(y-b_i)^2}\sqrt{x^2+y^2}}. \quad (34)$$

where $\{\mathbf{W}\}_{i,j}$ denotes the entry at the ith row and jth column.

From this we can see that $\mathbf{W} = \mathbf{U}$. Comparing (21) and (31), it follows

$$\mathrm{cov}(\hat{\mathbf{z}}) \approx \mathbf{J}^{-1}. \quad (35)$$

Then,

$$E[(\hat{x}-x)^2+(\hat{y}-y)^2] \approx \left\{\mathbf{J}^{-1}\right\}_{1,1} + \left\{\mathbf{J}^{-1}\right\}_{2,2}.$$

Therefore, the variance of the estimation error is the same as the CRLB.

In the following, we first employ an example to show that $[\hat{x},\hat{y}]$ obtained by TSE are Gaussian distributed with covariance matrix $\mathbf{J}^{-1}$, and then give the explanation for this phenomenon. Let the transmitter be at [0, 0], target at [0.699, 4.874] and four receivers at [-1, 1], [2, 1], [-3 1.1] and [4 0]. The signal travel distance variance at four receivers are $[0.1000, 0.1300, 0.1200, 0.0950]\times 10^{-4}$. The two dimensional probability density function (PDF) of $[\hat{x},\hat{y}]$ is shown in Fig. 4 (a). To verify the Gaussianity of $[\hat{x},\hat{y}]$, the difference between the PDF of $[\hat{x},\hat{y}]$ and the PDF of Gaussian distribution with mean $[\bar{x},\bar{y}]$ and covariance $\mathbf{J}^{-1}$ is plotted in Fig. 4 (b).

The Gaussianity of $[\hat{x},\hat{y}]$ can be explained as follows. Eqn. (35) means that the covariance of the final estimation of target location is the FIM related to CRLB. We could further study the distribution of $[e_x, e_y]$. The basic idea is that by omitting the second or high order and nonlinear errors, $[e_x, e_y]$ can be written as linear function of $\mathbf{e}$:

1) According to (29), $[e_x, e_y]$ are approximately linear transformations of $\hat{\Upsilon}$.
2) (15) means that $\hat{\Upsilon}$ is approximately a linear transformation of $\hat{\Theta}$. Here we could omit the nonlinear errors occurred in the estimate/calculation of $\mathbf{\Omega}$.
3) According to (11), $\hat{\Theta} \approx \bar{\theta}^2 + 2\bar{\theta}\mathbf{n} + \mathbf{n}^2$, thus, omitting the second order error, thus, $\hat{\Theta}$ is approximately a linear transformation of $\mathbf{n}$.
4) (10) and (39) mean that $\mathbf{n}$ is approximately a linear transformation of $\mathbf{e}$. Here we could omit the nonlinear errors accrued in the estimate of $\mathbf{S}$ and $\mathbf{\Psi}$.

Thus, we could approximately write $[e_x, e_y]$ as a linear transformation of $\mathbf{e}$, thus, $[e_x, e_y]$ can be approximated as Gaussian variables.

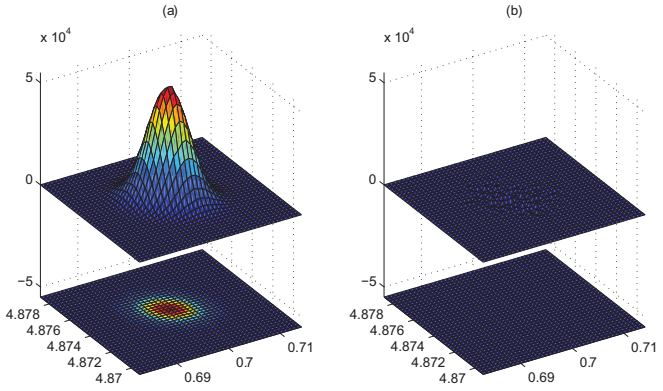

Fig. 4. (a): PDF of $[\hat{x},\hat{y}]$ by TSE (b): difference between the PDF of $[\hat{x},\hat{y}]$ by TSE and PDF of Gaussian distribution with mean $[\bar{x},\bar{y}]$ and covariance $\mathbf{J}^{-}1$.

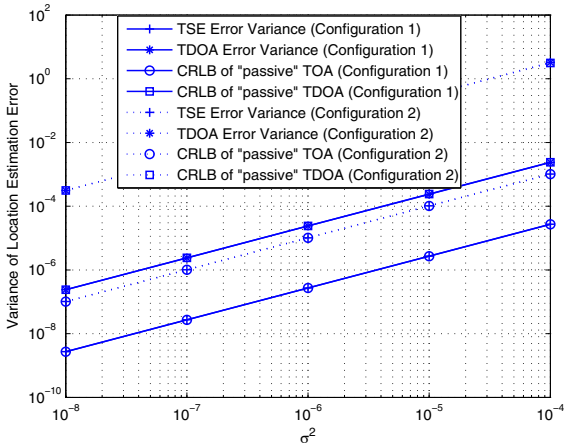

Fig. 5. Simulation results of TSE for the first configuration.

VI. Simulation Results

In this section, we first compare the performance of TSE with that TDOA algorithm proposed in [16] and CRLBs. Then, we show the performance of TSE at high TOA measurement error scenario. For comparison, the performance of a Quasi-Newton iterative method [35] is shown.

To verify our theoretical analysis, six different system configurations are simulated. The transmitter is at [0, 0] for all six configurations, and the receiver locations and error variances are listed in Table I. Figures 5, 6 and 7 show simulation results comparing the distance to the target (Configuration 1 vs. Configuration 2), the receiver separation (Configuration 3 vs. Configuration 4) and the number of receivers (Configuration 5 vs. Configuration 6), respectively [4]. In each figure, 10000 trails are simulated and the estimation variance of TSE estimate is compared with the CRLB of TDOA and TOA based localization schemes. For comparison, the simulation results of error variance of the TDOA method proposed in [16] are also drawn in each figure.

It can be observed that

1) The localization error of TSE can closely approach the CRLB of TOA based positioning algorithms.

[4]During the simulations, only one iteration is used for the calculation of $\mathbf{B}$ (19).

TABLE I
MEASUREMENT SYSTEM PARAMETERS

Configuration #	$[x, y]$	**Receivers Locations $[a_i, b_i]$ and TOA Error Variances**
1	[3, 8]	[-1, 1] ($0.1\sigma^2$), [2, 1] ($0.13\sigma^2$), [-3, 1.1] ($0.12\sigma^2$), [4, 0] ($0.095\sigma^2$)
2	[31, 28]	[-1, 1] ($0.1\sigma^2$), [2, 1] ($0.13\sigma^2$), [-3, 1.1] ($0.12\sigma^2$), [4, 0] ($0.095\sigma^2$)
3	[10, 13]	[-1, 1] ($1.0\sigma^2$), [1, 1] ($1.0\sigma^2$), [1, -1] ($1\sigma^2$), [-1, -1] ($1\sigma^2$)
4	[10, 13]	[-3, 3] ($1.0\sigma^2$), [3, 3] ($1.0\sigma^2$), [3, -3] ($1\sigma^2$), [-3, -3] ($1\sigma^2$)
5	[12, 8.5]	[-2.1, 3] ($0.5\sigma^2$), [1, 3.1] ($1.2\sigma^2$), [2.4, 5.1] ($1.0\sigma^2$), [-2.8, -1.6] ($0.9\sigma^2$)
6	[12, 8.5]	[-2.1, 3] ($0.5\sigma^2$), [1, 3.1] ($1.2\sigma^2$), [2.4, 5.1] ($1.0\sigma^2$), [-2.8, -1.6] ($0.9\sigma^2$), [-4, -2] ($0.7\sigma^2$), [2, 5] ($0.8\sigma^2$)

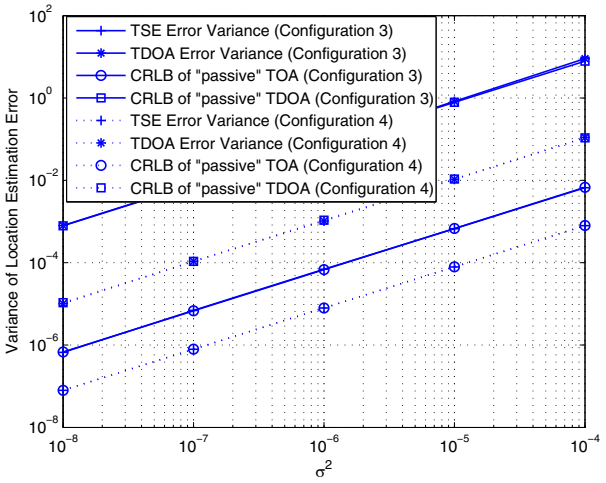

Fig. 6. Simulation results of TSE for the second configuration.

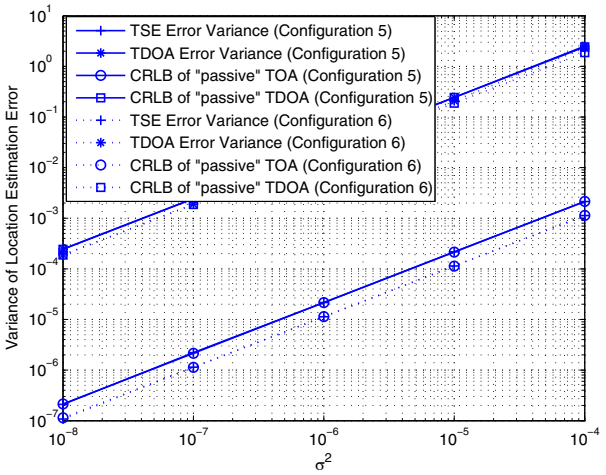

Fig. 7. Simulation results of combined TSE and TDOA algorithm for the third configuration.

2) The CRLB of TDOA based positioning algorithms is much higher (about 30dB for Configuration 3, 5 and 6) than that of TOA based.

Moreover, other interesting observations include

1) **Distance to Target**: Figure 5 shows that the target location estimate has larger error variance when the target is farther from the receivers.
2) **Receiver separation**: Fig. 6 shows that larger size of the receiver cluster leads to smaller location estimate error variance.
3) **Number of Receivers**: Fig. 7 shows that having more receivers achieves lower location estimate error variance.

Table II shows the performance of TSE with larger TOA measurement error covariance for Configuration 1 and 6. For comparison, we also show the performance of the Quasi-Newton method which numerically finds the maximum likelihood estimate of target location $[x, y]$ for $p(\hat{\mathbf{r}}|\mathbf{z})$ in (3). The Quasi-Newton method is performed by *fminunc* in MATLAB, using multiple rounds of iterations. The initial guess for the Quasi-Newton method $[\widetilde{x}, \widetilde{y}]$ satisfies that $\widetilde{x} - \bar{x}$ and $\widetilde{y} - \bar{y}$ are both Gaussain random variables with zero mean and variance 1 meter. The average numbers of iterations of Quasi-Newton are shown in the bracket after the values for the mean square estimation errors. Note that on the other hand, there is only one iteration for TSE in all simulations. Noteworthy observations are:

1) For small value of errors $\sigma < 0.5$, both TSE and Quasi-Newton approach the CRLB closely.
2) For large value of errors $\sigma > 0.5$, the TSE deviates from the CRLB since the second order errors are not negligible in this situation.

From the simulation results and previous analysis, we can observe the advantages of TSE over iterative methods are:

1) The computational complexity of TSE is much smaller than that of iterative methods , while both achieve the CRLB for small TOA measurement error. Thus, TSE is an ideal candidate for ultra-wideband TOA localization systems, which have better than centimeter accuracy [13].
2) The estimation result of TSE is predictable: the estimated target location is a Gaussian random variable with known covariance matrix. This feature is very help helpful when the estimated target location is further utilized [36].

VII. EXPERIMENTAL RESULTS

In this section, we apply the TSE algorithm to actual measurement results. In order to obtain reproducible results that show reduced impact of background and indirect paths, we place the target, an aluminum pole, in an anechoic chamber. The chamber, part of the UltraLab at the University of Southern California, exhibits very low wall reflectivity in the whole considered frequency range. Different materials have different properties for radio signal reflection. The aluminum pole in this experiment is used to obtain a good reflection of radio signals. There are several previous studies for positioning of objects with different materials, e.g., [28] and [13] studied the positioning of human body (chest movement), and [37] focused on the positioning of cancer inside human body.

TABLE II
COMPARISON BETWEEN TSE AND QUASI-NEWTON MINIMIZATION OF (3)

Configuration # (Method)	$\sigma = 0.01$	$\sigma = 0.036$	$\sigma = 0.1$	$\sigma = 0.3162$	$\sigma = 0.5623$
1 (CRLB of TOA)	$2.704 \cdot 10^{-5}$	$2.704 \cdot 10^{-4}$	$2.704 \cdot 10^{-3}$	$2.704 \cdot 10^{-2}$	$8.551 \cdot 10^{-2}$
1 (Quasi-Newton)	$2.707 \cdot 10^{-5}$ (8.4)	$2.708 \cdot 10^{-4}$ (8.4)	$2.765 \cdot 10^{-3}$(8.4)	$2.669 \cdot 10^{-2}$ (8.4)	$8.619 \cdot 10^{-2}$ (8.4)
1 (TSE)	$2.707 \cdot 10^{-5}$	$2.709 \cdot 10^{-4}$	$2.775 \cdot 10^{-3}$	$2.776 \cdot 10^{-2}$	$3.045 \cdot 10^{-1}$
6 (CRLB of TOA)	$1.137 \cdot 10^{-3}$	$1.137 \cdot 10^{-2}$	$1.137 \cdot 10^{-1}$	1.137	3.594
6 (Quasi-Newton)	$1.137 \cdot 10^{-3}$ (9.7)	$1.139 \cdot 10^{-2}$(9.7)	$1.158 \cdot 10^{-1}$(9.7)	1.1310(10.2)	5.801(11.3)
6 (TSE)	$1.137 \cdot 10^{-3}$	$1.137 \cdot 10^{-2}$	$1.180 \cdot 10^{-1}$	1.642	7.871

Figure 8 (a) shows the measurement setup. Transfer functions are measured by means of an 8720ET Agilent Vector Network Analyzer (VNA), which steps through 801 frequency points from 2 to 8 GHz. The transmit antenna is a UWB horn antenna with strong directionality and the receive antenna is a planar monopole UWB antenna with approximately omnidirectional radiation pattern designed using the Jumping Genes Multiobjective Optimization Scheme [38]. The directional antenna can achieve more accurate localization performance than the omnidirectional antenna, when the target direction is roughly known. For example, the directional antenna can point to the windows in the intruder detection system. In this experiment, we use the directional antenna for experimental convenience to enhance signal to interference noise ratio (SINR) and consequently achieve accurate TOA measurements. In the chamber, there is one transmitter, three sequentially measured receive antennas and an aluminum pole as the target. Figure 8 (b) shows the transmitter and the third receiver in the chamber.

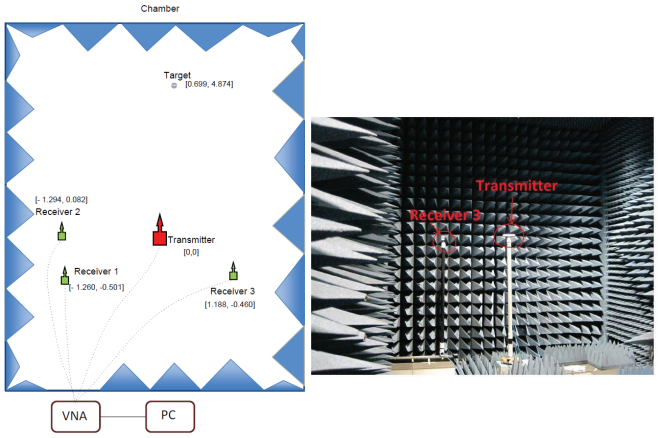

(a) Measurement Setup schematic (b) Pictures of transmitter and the third receiver

Fig. 8. Measurement setup schematic.

The transmit signals can propagate from the transmitter to the receiver either directly via the target (direct path), through paths that involve both the target and other object (indirect paths), or through paths that do not involve the target at all (background paths). In the first step, the background paths are eliminated through background subtraction [28]. We then subsequently use Maximum Likelihood parameter estimation, in particular the RIMAX algorithm [39], [13] to extract the TOAs from the transmitter to three receivers, respectively; we furthermore obtain the strengths, and thus the SNRs, of the direct paths at the receivers. The flow chart of target location estimation using TSE is shown in Figure 9. The measurement setup parameters are as follows:

- Transmitter Location: [0, 0] meter,
- Target Location: [0.699, 4.874] meter,
- Receiver 1 Location: [-1.260, -0.501] meter,
- Receiver 2 Location: [-1.294, 0.082] meter,
- Receiver 3 Location: [1.188, -0.460] meter,
- Tx and Rx frequency band: 2-8 Ghz,
- Transmitted signal power: -10 dbm.

From the TOA estimates, the target is localized using the TSE algorithm.

There are 100 triples of measured signal travel ranges $\hat{r}_1$, $\hat{r}_2$ and $\hat{r}_3$ at the three receivers, respectively, where $\hat{r}_i$ denotes the range measurement at the ith receiver. The mean values of $\hat{r}_1$, $\hat{r}_2$ and $\hat{r}_3$ are 10.645, 10.114 and 10.280 meters, respectively. The standard deviations of $\hat{r}_1$, $\hat{r}_2$ and $\hat{r}_3$ are 0.0015, 0.0012 and 0.0016 meters, respectively. The histogram plots of $\hat{r}_1$, $\hat{r}_2$ and $\hat{r}_3$ are shown in Fig. 10.

Based on the variance of $\hat{r}_1$, $\hat{r}_2$ and $\hat{r}_3$ and locations of the receivers, the CRLBs of TOA and TDOA algorithms are 1.65×10^{-5} m^2 and 0.0379 m^2 under the assumption of Gaussian distributions of $\hat{r}_1$, $\hat{r}_2$ and $\hat{r}_3$. The estimation error variance of the target location obtained with TSE is 1.73×10^{-5} m^2, while that of the TDOA based algorithm in [16] is 0.0340 m^2, respectively. Both the error variances of TSE and the TDOA algorithms are close to their CRLBs. However, the CRLB of TDOA is 2.3×10^3 times that of TOA. In other words, the estimation error variance of TSE is expected to be about 33 dB lower than the achievable error variance using TDOA based algorithms.

VIII. CONCLUSIONS

This paper proposes a novel algorithm, called TSE, for positioning of targets. In contrast to previous papers, it considers the case where the target is *not* the transmitter while at the same time transmitter and receivers are synchronized and can exploit the information of time-of-arrival (TOA), instead of the less-accurate time-difference of arrival (TDOA). The TSE proceeds in two steps, first computing estimates for a parameter set x, y, and $\sqrt{x^2+y^2}$, secondly updating the location vector $[x, y]$ from the results of first step.

By both theoretical analysis and numerical simulations, we show that for small TOA estimation errors the TSE approaches the CRLB very closely with only one iteration. Further results show the CRLB of passive TOA estimation to be much lower than that of TDOA. This indicates that the synchronization between the transmitter and the receivers can substantially decrease the localization error.

Experiments also showed that the error variance of TSE is very close to the CRLB of TOA algorithms under the

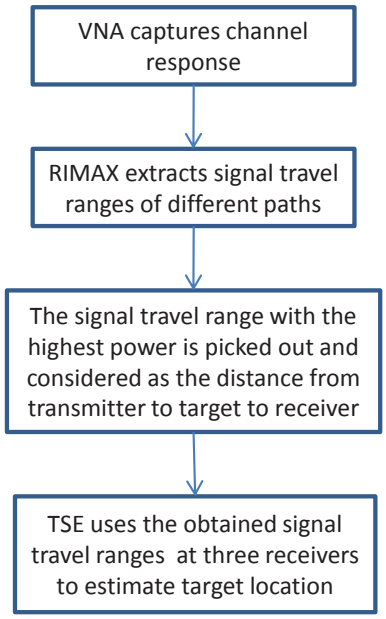

Fig. 9. Flow chart of target location estimation using TSE.

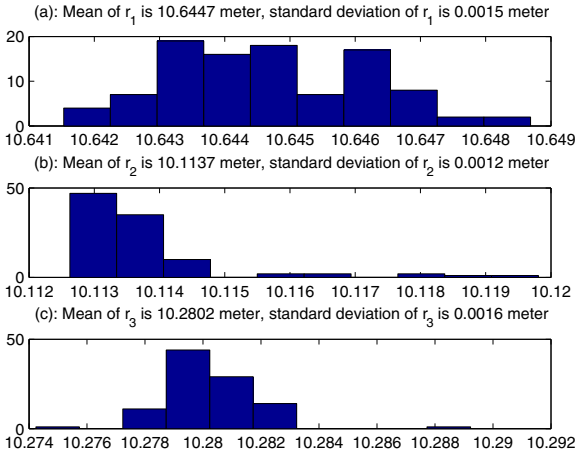

Fig. 10. Distribution of 100 measured signal travel ranges $\hat{r}_1$, $\hat{r}_2$ and $\hat{r}_3$ at three receivers.

assumption of Gaussian range measurement errors. In addition, the error variance of TSE is significantly (33 dB in our measurements) lower than that of TDOA algorithms.

Our results thus demonstrate the potential advantages of using synchronization between TX and RX in passive object localization, and furthermore provide a practical tool to exploit this potential to its full extent.

IX. Acknowledgements

The authors would like to thank Mr. Seun Sangodoyin and Dr. Xuesong Yang for their invaluable help during the measurement campaign.

Appendix
Proof of Lemma 1

Let $\hat{\boldsymbol{\theta}} = \bar{\boldsymbol{\theta}} + \mathbf{n}$, $\hat{\mathbf{S}} = \bar{\mathbf{S}} + \mathbf{e_S}$ and $\hat{\mathbf{h}} = \bar{\mathbf{h}} + \mathbf{e_h}$, where $\bar{\boldsymbol{\theta}}$, $\bar{\mathbf{S}}$ and $\bar{\mathbf{h}}$ are true/mean values and $\hat{\boldsymbol{\theta}}$, $\hat{\mathbf{S}}$ and $\hat{\mathbf{h}}$ are the measured/estimated values. Obviously,

$$\bar{\mathbf{h}} - \bar{\mathbf{S}}\bar{\boldsymbol{\theta}} = 0. \tag{36}$$

According to (5) and (7),

$$\begin{aligned} \boldsymbol{\varphi} &= \bar{\mathbf{h}} + \mathbf{e_h} - (\bar{\mathbf{S}} + \mathbf{e_S})\bar{\boldsymbol{\theta}} \\ &= \mathbf{e_h} - \mathbf{e_S}\bar{\boldsymbol{\theta}}. \end{aligned} \tag{37}$$

Multiplying both sides of (10) by $(\bar{\mathbf{S}}^T + \mathbf{e_S}^T)\boldsymbol{\Psi}^{-1}(\bar{\mathbf{S}} + \mathbf{e_S})$, it follows

$$\begin{aligned} &(\bar{\mathbf{S}}^T + \mathbf{e_S}^T)\boldsymbol{\Psi}^{-1}(\bar{\mathbf{S}} + \mathbf{e_S})(\bar{\boldsymbol{\theta}} + \mathbf{n}) \\ &= (\bar{\mathbf{S}}^T + \mathbf{e_S}^T)\boldsymbol{\Psi}^{-1}(\bar{\mathbf{h}} + \mathbf{e_h}), \end{aligned}$$

Leaving only the linear perturbation terms by omitting the second order errors, using (36), it follows that

$$\bar{\mathbf{S}}^T\boldsymbol{\Psi}^{-1}\bar{\mathbf{S}}\mathbf{n} \approx \bar{\mathbf{S}}\boldsymbol{\Psi}^{-1}(\mathbf{e_h} - \mathbf{e_S}\bar{\boldsymbol{\theta}}).$$

Then, we obtain

$$\begin{aligned} \mathbf{n} &= (\bar{\mathbf{S}}^T\boldsymbol{\Psi}^{-1}\bar{\mathbf{S}})^{-1}\bar{\mathbf{S}}\boldsymbol{\Psi}^{-1}(\mathbf{e_h} - \mathbf{e_S}\bar{\boldsymbol{\theta}}) \\ &= (\bar{\mathbf{S}}^T\boldsymbol{\Psi}^{-1}\bar{\mathbf{S}})^{-1}\bar{\mathbf{S}}\boldsymbol{\Psi}^{-1}\boldsymbol{\varphi}. \end{aligned} \tag{38}$$

According to (5) and (7), substitute $\boldsymbol{\varphi}$ by $\mathbf{Be}$, it follows that

$$\mathbf{n} \approx (\bar{\mathbf{S}}^T\boldsymbol{\Psi}^{-1}\bar{\mathbf{S}})^{-1}\bar{\mathbf{S}}\boldsymbol{\Psi}^{-1}\mathbf{Be}. \tag{39}$$

Then,

$$\begin{aligned} cov(\hat{\boldsymbol{\theta}}) &\approx E(\mathbf{n}\mathbf{n}^T) \\ &= (\bar{\mathbf{S}}^T\boldsymbol{\Psi}^{-1}\bar{\mathbf{S}})^{-1}\bar{\mathbf{S}}^T\boldsymbol{\Psi}^{-1}\mathbf{B}E(\mathbf{e}\mathbf{e}^T) \\ &\quad \times\mathbf{B}^\mathbf{T}\boldsymbol{\Psi}^{-\mathbf{1}}\bar{\mathbf{S}}[(\bar{\mathbf{S}}^T\boldsymbol{\Psi}^{-1}\bar{\mathbf{S}})^{-1}]^T. \end{aligned}$$

Because $\mathbf{B}E(\mathbf{e}\mathbf{e}^T)\mathbf{B}^\mathbf{T} = \boldsymbol{\Psi}$, and $[(\bar{\mathbf{S}}^T\boldsymbol{\Psi}^{-1}\bar{\mathbf{S}})^{-1}]^T = (\bar{\mathbf{S}}^T\bar{\boldsymbol{\Psi}}^{-1}\bar{\mathbf{S}})^{-1}$, it follows that

$$\begin{aligned} cov(\hat{\boldsymbol{\theta}}) &\approx (\bar{\mathbf{S}}^T\boldsymbol{\Psi}^{-1}\bar{\mathbf{S}})^{-1}\bar{\mathbf{S}}^T\boldsymbol{\Psi}^{-1}\bar{\mathbf{S}}(\bar{\mathbf{S}}^T\boldsymbol{\Psi}^{-1}\bar{\mathbf{S}})^{-1} \\ &= (\bar{\mathbf{S}}^T\boldsymbol{\Psi}^{-1}\bar{\mathbf{S}})^{-1}, \end{aligned}$$

which ends the proof of Lemma 1.

References

[1] N. Patwari and J. Wilson, "RF sensor networks for device-free localization: measurements, models, and algorithms," *Proc. IEEE*, vol. 98, no. 11, pp. 1961–1973, 2010.

[2] A. Ko and H. Lau, "Robot assisted emergency search and rescue system with a wireless sensor network," *Int'l J. Advanced Sci. and Technol.*, vol. 3, pp. 69–78, 2009.

[3] C. Hekimian-Williams, B. Grant, X. Liu, Z. Zhang, and P. Kumar, "Accurate localization of RFID tags using phase difference," in *Proc. 2010 IEEE International Conference on RFID*, pp. 89–96.

[4] C. Debono and E. Sammut, "Location estimation of an intruder in wireless ad hoc networks," in *Proc. 2008 IEEE Mediterranean Electrotechnical Conference*, pp. 158 –162.

[5] A. Weiss, "On the accuracy of a cellular location system based on RSS measurements," *IEEE Trans. Veh. Technol.*, vol. 52, no. 6, pp. 1508–1518, Nov. 2003.

[6] Y. Zhu, D. Huang, and A. Jiang, "Network localization using angle of arrival," in *Proc. 2008 IEEE International Conference on Electro/Information Technology*, pp. 205–210.

[7] S. Gezici, Z. Tian, G. Giannakis, H. Kobayashi, A. F. Molisch, H. Poor, and Z. Sahinoglu, "Localization via ultra-wideband radios: a look at positioning aspects for future sensor networks," *IEEE Signal Process. Mag.*, vol. 22, no. 4, pp. 70–84, July 2005.

[8] I. Guvenc and C.-C. Chong, "A survey on TOA based wireless localization and NLOS mitigation techniques," *IEEE Commun. Surveys & Tutorials*, vol. 11, no. 3, pp. 107–124, 2009.

[9] J. Xu, M. Ma, and C. Law, "Position estimation using UWB TDOA measurements," in *Proc. 2006 IEEE International Conference on Ultra-Wideband*, pp. 605–610.
[10] Y. Shen and M. Win, "On the accuracy of localization systems using wideband antenna arrays," *IEEE Trans. Commun.*, vol. 58, no. 1, pp. 270–280, Jan. 2010.
[11] K. Yu, J. Montillet, A. Rabbachin, P. Cheong, and I. Oppermann, "UWB location and tracking for wireless embedded networks," *Signal Process.*, vol. 86, no. 9, pp. 2153–2171, 2006.
[12] R. Zetik, J. Sachs, and R. Thoma, "UWB short-range radar sensing—the architecture of a baseband, pseudo-noise UWB radar sensor," *IEEE Instrumentation Measurement Mag.*, vol. 10, no. 2, pp. 39–45, Apr. 2007.
[13] J. Salmi and A. Molisch, "Propagation parameter estimation, modeling and measurements for ultrawideband MIMO radar," *IEEE Trans. Antennas Propag.*, vol. 59, no. 11, pp. 4257–4267, Nov. 2011.
[14] J. Zhang, P. Orlik, Z. Sahinoglu, A. F. Molisch, and P. Kinney, "UWB systems for wireless sensor networks," *Proc. IEEE*, vol. 97, no. 2, pp. 313–331, 2009.
[15] C.-C. Chui and R. Scholtz, "Time transfer in impulse radio networks," *IEEE Trans. Commun.*, vol. 57, no. 9, pp. 2771–2781, 2009.
[16] Y. Chan and K. Ho, "A simple and efficient estimator for hyperbolic location," *IEEE Trans. Signal Process.*, vol. 42, no. 8, pp. 1905–1915, 1994.
[17] Y.-T. Chan, H. Yau Chin Hang, and P.-C. Ching, "Exact and approximate maximum likelihood localization algorithms," *IEEE Trans. Veh. Technol.*, vol. 55, no. 1, pp. 10–16, Jan. 2006.
[18] K. Cheung, H. So, W.-K. Ma, and Y. Chan, "Least squares algorithms for time-of-arrival-based mobile location," *IEEE Trans. Signal Process.*, vol. 52, no. 4, pp. 1121–1130, Apr. 2004.
[19] M. Youssef, M. Mah, and A. Agrawala, "Challenges: device-free passive localization for wireless environments," in *Proc. 2007 ACM International Conference on Mobile Computing and Networking*, pp. 222–229. Available: http://doi.acm.org/10.1145/1287853.1287880
[20] A. Athalye, V. Savic, M. Bolic, and P. Djuric, "A radio frequency identification system for accurate indoor localization," in *Proc. 2011 IEEE International Conference on Acoustics, Speech and Signal Processing*, pp. 1777–1780.
[21] I. Jouny, "Blind source separation for extraction of target scattering centers," in *Proc. 2006 IEEE Antennas and Propagation Society International Symposium*, pp. 1291–1294.
[22] M. Poh, D. McDuff, and R. Picard, "Non-contact, automated cardiac pulse measurements using video imaging and blind source separation," *Opt. Express*, vol. 18, no. 10, pp. 10 762–10 774, 2010.
[23] J. Shen and A. Molisch, "Discerning direct and indirect paths: principle and application in passive target positioning systems," in *Proc. 2011 IEEE Global Telecommunications Conference*, pp. 1–6.
[24] S. Marano and, W. M. Gifford, H. Wymeersch, and M. Z. Win, "NLOS identification and mitigation for localization based on UWB experimental data," *IEEE J. Sel. Areas Commun.*, vol. 28, no. 7, pp. 1026–1035, 2010.
[25] K. Ho and W. Xu, "An accurate algebraic solution for moving source location using tdoa and fdoa measurements," *IEEE Trans. Signal Process.*, vol. 52, no. 9, pp. 2453–2463, Sep. 2004.
[26] H. Godrich, A. Haimovich, and R. Blum, "Target localization accuracy gain in MIMO radar-based systems," *IEEE Trans. Inf. Theory*, vol. 56, no. 6, pp. 2783–2803, 2010.
[27] X. Zhang, P. Willett, and Y. Bar-Shalom, "Monopulse radar detection and localization of multiple unresolved targets via joint bin processing," *IEEE TRans. Signal Process.*, vol. 53, no. 4, pp. 1225–1236, Apr. 2005.
[28] J. Salmi, S. Sangodoyin, and A. F. Molisch, "High resolution parameter estimation for ultra-wideband MIMO radar," in *Proc. 2010 Asilomar Conference on Signals, Systems, and Computers*.
[29] L. Carlone, R. Aragues, J. A. Castellanos, and B. Bona, "A linear approximation for graph-based simultaneous localization and mapping," in *Robotics: Science and Systems*, 2011.
[30] J. Spilker, *The Global Positioning System: Theory and Applications, Vol. 2*. Aiaa, 1996.
[31] H. Van Trees, K. Bell, and Y. Wang, "Bayesian Cramer-Rao bounds for multistatic radar," in *Proc. 2006 IEEE Int. Waveform Diversity Design Conf.*
[32] G. Shi and A. Nehorai, "Cramer-Rao bound analysis on multiple scattering in multistatic point scatterer estimation," in *Proc. 2006 IEEE International Conference on Acoustics, Speech and Signal Processing*, vol. 4, p. IV.
[33] M. Greco, P. Stinco, F. Gini, and A. Farina, "Cramer-Rao bounds and selection of bistatic channels for multistatic radar systems," *IEEE TRans. Aerospace and Electron. Syst.*, vol. 47, no. 4, pp. 2934–2948, Oct. 2011.
[34] S. M. Kay, *Fundamentals of Statistical Signal Processing*. Prentice-Hall, Inc., 1993.
[35] J. Nocedal and S. Wright, *Numerical Optimization*. Springer Verlag, 1999.
[36] H. Luecken and A. Wittneben, "UWB radar imaging based multipath delay prediction for NLOS position estimation," in *2011 IEEE International Conference on Ultra-Wideband*.
[37] M. Klemm, I. Craddock, J. Leendertz, A. Preece, and R. Benjamin, "Radar-based breast cancer detection using a hemispherical antenna array experimental results," *IEEE TRans. Antennas and Propag.*, vol. 57, no. 6, pp. 1692–1704, June 2009.
[38] X. Yang, K. Ng, S. Yeung, and K. Man, "Jumping genes multiobjective optimization scheme for planar monopole ultrawideband antenna," *IEEE Trans. Antennas Propag.*, vol. 56, no. 12, pp. 3659–3666, 2008.
[39] A. Richter, "Estimation of radio channel parameters: models and algorithms," Ph. D. dissertation, Technischen Universität Ilmenau, Germany, May 2005, ISBN 3-938843-02-0.

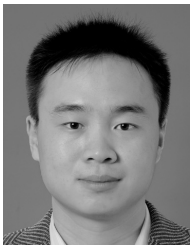

Junyang Shen (S'08) received the B.S. degree from Huazhong University of Science and Technology, China, in 2006 and the M.S. degree (Hon.) from Beijing University of Posts and Technology, China, in 2009. Since Aug. 2009, he worked toward the Ph.D. degree with the Department of Electrical and Engineering, University of Southern California, Los Angeles. He has researched on spectrum sensing in Cognitive Radio. Now, His research interests cover MIMO radar, UWB location and monitoring.

He has served as a Technical Program Committee (TPC) member for the IEEE International Conference on Communications (ICC) in 2012. He received the Best Student Paper Award in IEEE International Conference on Ultra-Wideband (ICUWB), 2011.

Andreas F. Molisch (S'89, M'95, SM'00, F'05) is Professor of Electrical Engineering at the University of Southern California, Los Angeles, CA, USA. Previously, he was with AT&T (Bell) Laboratories Research (USA), Lund University (Sweden), Mitsubishi Electric Research Labs, (USA), and TU Vienna (Austria).

Dr. Molisch's current research interests are measurement and modeling of mobile radio channels, UWB communications and localization, cooperative communications, MIMO systems, advanced cellular architectures, and wireless systems for healthcare. He has authored, coauthored or edited four books (among them the textbook *Wireless Communications* (Wiley-IEEE Press), fourteen book chapters, more than 140 journal papers, and numerous conference contributions, as well as more than 70 patents and 60 standards contributions.

Dr. Molisch has been an editor of a number of journals and special issues, General Chair, TPC Chair, or Symposium Chair of multiple international conferences, and chairman of various international standardization groups. He is a Fellow of the IEEE, a Fellow of the IET, an IEEE Distinguished Lecturer, and a member of the Austrian Academy of Sciences. He is the recipient of numerous awards, most recently the Donald Fink Prize of the IEEE and the Eric Sumner Award of the IEEE.

Jussi Salmi (S'05-M'09) was born in Finland in 1981. He received the M.Sc. and D.Sc. degrees, both with honors, from Helsinki University of Technology (HUT), Finland, in 2005 and 2009, respectively. In 2009-2010 he worked as a Postdoctoral Research Associate in the Department of Electrical Engineering, University of Southern California, Los Angeles, CA. Currently, he works as a Postdoctoral researcher in the Department of Signal Processing and Acoustics, Aalto University School of Electrical Engineering (former HUT), Finland. His current research interests include RF-based vital sign detection, UWB MIMO radar, indoor positioning, measurement based MIMO channel modeling, and parameter estimation. He is the author of over 30 research papers in international journals and conferences. Dr. Salmi received the Best Student Paper Award in EUSIPCO'06, and co-authored a paper receiving the Best Paper Award in Propagation in EuCAP'06.